Epitaxial BiFeO3 multiferroic thin film heterostructures

Wang, J.; Neaton, J. B.; Zheng, H.; Nagarajan, V.; Ogale, S. B.; Liu, B.; Viehland, D.; Schlom, D. G.; Waghmare, U. V.; Spaldin, N. A.; Rabe, K. M.; Wuttig, M.; Ramesh, R.

2003

Wang, J., Neaton, J. B., Zheng, H., Nagarajan, V., Ogale, S. B., Liu, B., & et al. (2003). Epitaxial BiFeO3 Multiferroic Thin Film Heterostructures. Science, 299(5613), 1719-1722.

https://hdl.handle.net/10356/99744

https://doi.org/10.1126/science.1080615

Epitaxial $BiFeO_3$ Multiferroic Thin Film Heterostructures

J. Wang[1*], J. B. Neaton[2†], H. Zheng[1†], V. Nagarajan[1], S. B. Ogale[3], D. Viehland [4], V.Venugopalan[5], D.G. Schlom[5], U. V. Waghmare[6], N. A. Hill[7], and K. M. Rabe[2], M. Wuttig[1], and R. Ramesh[3]

[1]Department of Materials Science and Engineering and [3] Department of Physics

University of Maryland, College Park, MD 20742

[2] Department of Physics and Astronomy, Rutgers University, Piscataway, NJ 08854

[4]Department of Materials Science and Engineering

Virginia Tech, Blacksburg, VA 24061

[5]Department of Materials Science and Engineering

Pennsylvania State University, University Park, PA 16802-5055

[6]J. Nehru Centre for Advanced Scientific Research, Jakkur, Bangalore 560 064 INDIA

[7] Materials Department, University of California, Santa Barbara, CA 94805

†These authors contributed equally to this work.

Abstract

Enhancement of polarization and related properties in heteroepitaxially constrained thin films of the ferroelectromagnet, $BiFeO_3$ is reported. Structure analysis indicates that the crystal structure is monoclinic in contrast to bulk, which is rhombohedral. The films display a room-temperature spontaneous polarization (50-60μC/cm^2) almost an order of magnitude higher than that of the bulk (6.1μC/cm^2). The observed enhancement is corroborated by first-principles calculations and found to originate from large relative displacements of the Bi, Fe, and O sublattices. The films also exhibit enhanced thickness-dependent magnetism compared with the bulk. These

enhanced and combined functional responses in thin film form present an exciting opportunity to create and implement novel thin film devices that actively couple the magnetic and ferroelectric order parameters.

Materials that have strong coupling between the electric, magnetic and structural order parameters, resulting in simultaneous ferroelectricity, ferromagnetism, and ferroelasticity, are known as multiferroics ***(1, 2)***. These compounds present exciting opportunities for potential applications in information storage, the emerging field of spintronics and sensors. There has been recent research interest in a number of prototypical magnetic ferroelectrics, including $YMnO_3$, a hexagonal perovskite that is antiferromagnetic (Neél temperature, T_N=70-130K) and ferroelectric (Curie temperature, T_C=570-990K) in the ground state ***(3, 4***), and $BiMnO_3$, a monoclinic perovskite which is both ferromagnetic (T_N~100K) and ferroelectric (T_C~450K) ***(5, 6, 7)***. The perovskite $BiFeO_3$ is ferroelectric (T_C~1103K) and antiferromagnetic (T_N~643K), exhibiting weak magnetism at room temperature due to a residual moment from a canted spin structure ***(2)***. The structure and properties of the bulk single crystal form have been extensively studied ***(8-12, 23)***, where it has been shown to possess a rhombohedrally distorted perovskite structure (a=b=c=5.63Å, α=β=γ=59.4˚) at room temperature. In single crystals, the spontaneous polarization (P_s) is 3.5μC/cm^2 along the (001) direction, indicating a value of 6.1μC/cm^2 along the (111) direction at 77K ***(10)***. Transport measurements in the bulk have been hampered by leakage problems, likely due to defects and non-stoichiometry, which have limited applications of this material. To overcome this, recent work has focused on solid solutions of $BiFeO_3$ with other ABO_3 (A is the cation at the vertices of the cube, B is the cation at the body center.) materials, such as $BaTiO_3$, which can prevent second phase formation and increase sample resistivity. For example, K. Ueda et al reported a remanent polarization of 2.5μC/cm^2 from $(Bi_{0.7}Ba_{0.3})(Fe_{0.7}Ti_{0.3})O_3$ film ***(13)***.

An important aspect that emerges upon examination of the properties of bulk $BiFeO_3$ (single crystal or ceramic) is that the parent compound has a spontaneous polarization value that is significantly smaller than what would normally be expected for a ferroelectric with such a high Curie temperature (for example, lead titanate, with a Tc of ~763K has a spontaneous polarization of 80-100$\mu C/cm^2$.) Indeed, this anomalous behavior has been noted in an earlier report ***(10)***. It is not clear whether this is due to intrinsic material properties or due to limitations imposed by leakage and imperfect material quality in bulk. The resolution of this issue was the initial motivation of this study, which focuses on creating a model thin film $BiFeO_3$ system via oxide heteroepitaxy.

In our experiments, we grew phase-pure $BiFeO_3$ (BFO) thin films in the thickness range of 50-500nm by pulsed laser deposition (PLD) onto single crystal $SrTiO_3$(100) (STO) substrates. To ensure heteroepitaxial growth, we chose the conducting perovskite oxide electrode, $SrRuO_3$ (SRO) ***(14)***. **(Details of growth and characterization can be found in SOM.)**

Large angle x-ray scans (20-80 degrees) showed only diffraction peaks from the substrate and (00l) pseudo-cubic reflections from the heterostructure. We did not observe any reflections that would be indicative of second phases. Fig.1A shows a small section of the x-ray diffraction spectra from films of varying thickness, demonstrating the dependence of the BFO out-of-plane lattice parameter on film thickness (cf. Fig. 2D). Selected area electron diffraction (SAED) patterns (Fig.1B), as well as low magnification bright field images, obtained from a (100) cross-section confirm the single crystalline quality of the BFO layer. Analysis of the SAED pattern reveals that the (010) and (001)

reflections have different spacings, yielding a ratio of 1.016. Indexing of this SAED pattern with pseudo-cubic indices yields an in-plane parameter of 3.935Å and an out-of-plane parameter of 4.0 Å. Careful analyses of the crystal structure using four-circle x-ray diffraction suggests a tetragonal-like crystal structure with the c-axis normal to the substrate surface, with a small monoclinic distortion of about 0.5º. These experimental observations can be interpreted as a consequence of a compressive stress imposed by the SRO electrode, which has an in-plane lattice parameter smaller than that of BFO. These results lead to two key observations: (i) heteroepitaxial, in-plane compressive stress imposed by the epitaxial bottom electrode allows growth of a monoclinic crystal structure in BFO and, (ii) the degree of compressive stress progressively decreases with increasing BFO thickness (as expected).

We probed the impact of this constrained crystallographic state in the BFO layer on its physical properties. Ferroelectric properties were characterized using both polarization hysteresis as well as pulsed polarization measurements. In the hysteresis loop measured at a frequency of 15kHz for the 200nm thick film (Fig.2A), the observed remanent polarization (Pr, 50-60μC/cm^2) is an order of magnitude higher than the highest reported value of 6.1μC/cm^2 from bulk BFO. To confirm this result, we measured the polarization characteristics under pulsed probe condition, which is less likely to be convoluted by leakage and nonlinear dielectric effects. The pulsed remanent polarization, (defined as $\Delta P=P^*-P^{\wedge}\approx 2P_r$ where P* is the switched polarization and P^ is the non-switched polarization) vs. applied electric field, measured using 10μsec wide pulses (Fig.2B) shows a sharp increase of ΔP around 15MV/m reaching a value of about 100μC/cm^2 at 55MV/m. The films display resistivity values of ~10^9Ω.cm, which is

comparable with values obtained for epitaxial Ti-rich lead zirconate titanate (PZT) films**.** This polar state was found to be stable, as evidenced by polarization retention experiments conducted over several days. Additional support for the spontaneous polar state comes from piezoelectric measurements. The piezoelectric hysteresis loop (Fig.2C), measured using a scanning force microscope (**Details of technique can be found in SOM)**, shows a remanent out-of-plane piezoelectric coefficient (d_{33}) value of 70pm/V, representing the piezoresponse of the film in the fully clamped state and is comparable to that obtained from Ti-rich PZT films (Zr/Ti ratio of 20/80) ***(15)*****.** Fig.2D summarizes the thickness dependence of the polarization and piezoelectric coefficient. While the polarization increases with reducing film thickness, the d_{33} value decreases. The small signal out-of-plane dielectric constant (ε_{33}), follows the same trend as the d_{33} measurements. In the case of epitaxial $PbTiO_3$ and $BaTiO_3$ films, in-plane compressive stresses lead to a decrease of ε_{33}, along with an enhancement of the spontaneous polarization ***(16)***. The thickness dependence observed in Fig.2D can be similarly understood as a direct consequence of the induced compressive stress imposed by heteroepitaxy.

To understand the experimental data at the atomic level, we turned to first principles calculations of total energy and polarization. These calculations were carried out within a local spin-density approximation (LSDA) with a plane wave basis set and projector augmented wave pseudopotentials using the Vienna Ab-initio Simulation Package (VASP) ***(17, 18)***. (All calculations have been verified with another plane wave-pseudopotential package, ABINIT ***(19)***.) For a number of ferroelectric oxides, the spontaneous polarization has been accurately computed from first principles ***(20)*** using

the Berry-phase formalism ***(21, 22)***. Specifically, this determines a discrete set of allowed values for the electronic contribution to the polarization $\mathbf{P}_{el}+2e\mathbf{R}/\Omega$, where **R** is a lattice vector, Ω is the unit cell volume, and *e* is the charge of the electron. The possible values for the change in polarization with switching (equal to twice the spontaneous polarization) are then $2\mathbf{P}_0+2e\mathbf{R}/\Omega$. Bellow, we report as the spontaneous polarization a single choice for $\mathbf{P}_0$ parallel to a given direction.

We first investigated the bulk rhombohedral phase by optimizing the structural parameters of $BiFeO_3$ in a 10-atom unit cell with space group R3c (Fig.3C). The structure can be described as a distorted perovskite. The ground state is found to be an antiferromagnetic insulator with a lattice constant of 5.459 Å and a rhombohedral angle of 60.36°, to be compared with the experimental values 5.6343 Å and 59.348° ***(23)***, deviations typical of the LSDA. The absence of centrosymmetry in R3c permits the relative displacements of the atomic sublattices along (111), most notably those of Bi with respect to the distorted FeO_6 cages, and the minimum energy structure has values of these displacements in excellent agreement with experimental structural determinations. The Berry-phase calculation yields a spontaneous polarization $\mathbf{P}_0 = +6.61\mu C/cm^2$ along (111), in excellent agreement with the reported bulk value of $6.1\mu C/cm^2$.

For the thin-film phase, we considered a tetragonal structure based on the cubic perovskite structure with symmetry lowered to *P*4*mm* (i.e., we ignored the small monoclinic distortion). The lattice parameters were fixed to the pseudo-tetragonal parameters measured for the 200nm film (a=3.935Å and c/a=1.016). Computations were performed with a body-centered tetragonal unit cell, doubled to accommodate the G-type antiferromagnetic ordering. The key results of our calculations for the thin film are shown

in Fig.3C,D. The magnitudes of the ionic displacements relative to the centrosymmetric strained perovskite structure were found to be extremely large: relative to the Bi ion, the Fe (Wyckoff position 4b) and apical O (4b) are displaced by about 9% (of the c-axis parameter) and 13%, respectively, and the equatorial O atoms (8c) by nearly 18%. (Fig.3C is a schematic tetragonal $BiFeO_3$ unit cell.) The Fe displacement along the Fe-O(4b) chain is negligible, while the oxygen octahedron is distorted by relative displacement of the equatorial and apical oxygens. The Berry-phase calculation yields a spontaneous polarization of +63.2 $\mu C/cm^2$ along (001), which is consistent with the experimentally observed large values of polarization of our (001) oriented films. While there may be other tetragonal structures lower in energy (the energy per unit cell is around 0.4eV per formula unit greater than the optimized rhombohedral structure), this result proves that a dramatically different polarization can be obtained with a relatively small change in the lattice parameters.

The results demonstrate the influence of heteroepitaxial constraint on the crystal structure and ferroelectric responses in the BFO thin film. We now turn our attention to the magnetic response. The field dependent magnetization is shown for a 70nm thick film (Fig.4). The inset (a) shows the thickness dependence of the magnetization. For the thinnest film that we have measured (70nm) the saturation magnetization is ~150emu/cc (corresponding to ~1μ_B per unit cell), as film thickness goes up to 400nm, magnetization decreases to ~5emu/cc. The films exhibit enhanced magnetization values compared to the bulk ceramic ***(24)*** although the lack of any published data on single crystal precludes any detailed comparative evaluation. The observation of a clear thickness dependence of the magnetization points to the effect of mismatch strain on the magnetic response. The

coupling of electric and magnetic orders in BFO type multiferroic gives rise to a magnetoelectric (ME) effect. A quasi-static setup ***(25)*** was used to determine the ME *dE/dH* coefficient of the epitaxial films. Preliminary result, shown in the inset (b), indicates a *dE/dH* coefficient as high as 3V/cm.Oe at zero field.

Our work presents direct experimental evidence for the heteroepitaxial stabilization of a monoclinic phase with large spontaneous polarization in the ferroelectromagnet system, $BiFeO_3$. These films also show a significant enhancement of magnetization compared to the bulk. A strong piezoelectric response of ~70pm/V provides the basis for creating lead-free piezoelectrics for sensors and actuators.

References and notes

1. E. K. H. Salje, Cambridge University, 1990.

2. G. A. Smolenskii, I. Chupis, Sov. Phys. Usp. 25, 475 (1982).

3. A. Filippetti, N. A. Hill, J. Magn. Magn. Mater. 236, 176 (2001).

4. M. Fiebig, Th. Lottermoser, D. Frohlich, A. V. Goltsev, R. V. Pisarev, Nature 419, 818 (2002).

5. N. A. Hill, K. M. Rabe, Phys. Rev. B 59, 8759 (1999).

6. R. Seshadri, N.A. Hill, Chem. Mat. 13, 2892 (2001).

7. A. M. dos Santos, S. Parashar, A. R. Raju, Y.S.Zhao, A. K. Cheetham, C. N. R Rao, Sol. Stat. Comm. 122, 49 (2002).

8. C. Michel, J-M.Moreau, G. D. Achenbach, R. Gerson, W. J. James, Solid State Commun. 7, 701 (1969).

9. J. D. Bucci, B. K. Robertson, W. J. James, J. Appl. Cryst. 5, 187 (1972).

10. J. R. Teague, R. Gerson, W. J. James, Solid State Commun. 8, 1073 (1970).

11. Yu. E. Roginskaya, Yu. Ya. Tomashpol'skii, Yu. N. Venevtsev, V. M. Petrov, G. S. Zhdanov, Sov. Phys. JETP 23, 47 (1966).

12. S. V. Kiselev, R. P. Ozerov, G. S. Zhdanov, Sov. Phys. Dokl. 7, 742 (1963).

13. K. Ueda, H.Tabata, T. Kawai, App. Phys. Lett. 75, 555 (1999).

14. C. B. Eom, R. J. Cava, R. M. Fleming, J.M. Phillips, Science 258, 1766 (1992).

15. M. J. Haun, E. Furman, S. J. Jang, L. E. Cross, Ferroelectrics 99, 63 (1989).

16. N. A. Pertsev, A. G. Zembilgotov, A. K. Tagantsev, Phys. Rev. Lett. 80, 1988 (1998).

17. G. Kresse, J. Hafner, Phys. Rev. B 47, 558 (1993); Phys. Rev. B 54, 11169 (1996).

18. G. Kresse, J. Joubert, Phys. Rev. B 59, 1758 (1999).

19. The ABINIT code is a common project of the Universite Catholique de Louvain, Corning Incorporated, and other contributors (URL http://www.abinit.org). See "First-principles computation of material properties: the ABINIT software project", X. Gonze et al, Comp. Mat. Sci. 25, 478 (2002).

20. See, for example, W. Zhong, R. D. King-Smith, D. Vanderbilt, Phys. Rev. Lett. 72, 3618 (1994).

21. R. D. King-Smith, D. Vanderbilt, Phys. Rev. B 47, 1651 (1993).

22. D. Vanderbilt and R. D. King-Smith, Phys. Rev. B 48, 4442 (1993).

23. F. Kubel, H. Schmid, Acta. Cryst. B 46, 698 (1990).

24. M. Mahesh Kumar, S. Srinath, G.S. Kumar, S. B. Suryanarayana, J. Magn. Magn. Mater. **188**, 203 (1998).

25. H. G. Rajaram, Ph.D. Thesis, Pennsylvania State University, 1991.

26. We thank B. Liu, L. V. Saraf and V. Kulkarni for help with XRD and RBS measurements. J. B. Neaton and K. M. Rabe thank D. Vanderbilt for useful discussions. This work is supported by the Office of Naval Research MURI N000140110761 and the National Science Foundation MRSEC DMR-00-80008. It also benefits from the support of the National Science Foundation grant DMR0095166.

List of figure captions

Fig.1 (A) (003) peaks from X-ray θ-2θ scans showing the effect of film thickness on heteroepitaxial strain. As the film thickness is increased from 70nm to 400nm, the peak position progressively increases ( : 70nm ; : 100nm ; : 200nm and : 400nm), indicating a decrease of the out-of-plane lattice parameter; (B) selected area electron diffraction pattern confirms the structure distortion.

Fig.2 (A) Ferroelectric hysteresis loop measured at a frequency of 15kHz, which shows that the film is ferroelectric with Pr ~55μC/cm^2. (B) Pulsed polarization, ΔP vs. electric field, measured with electrical pulses of 10μsec width; (C) small signal d_{33} for a 50μm capacitor and (D) summary of thickness dependence of out-of-plane lattice parameter, polarization and d_{33}. The small signal dielectric constant (not shown) follows the same trend as the d_{33}.

Fig.3 Schematic of the prototypical rhombohedral (A), and tetragonal (B) $BiFeO_3$ unit cells (Note that computations were performed with a ten-atom body-centered tetragonal unit cell, doubled to accommodate the G-type antiferromagnetic ordering). The corresponding atomic positions and spontaneous polarizations from first-principles calculations are shown in the tables (C) and (D) respectively. The asterisks in Fig.3 (D) indicate that lattice parameters were fixed to the experimental values of the 200nm film.

Fig.4 Magnetic hysteresis loops measured by vibrating sample magnetometry for a 70nm thick BFO film, showing an appreciable saturation magnetization of ~150emu/cc and a coercive field of ~200Oe. The in-plane loop is shown in blue and the out-of-plane loop is in red. Inset (a) shows the thickness dependence of saturation magnetization, illustrating the effect of heteroepitaxial constraint, and (b) is a preliminary ME measurement result showing a maximum value of ~3V/cm.Oe and hysteresis around 200Oe.

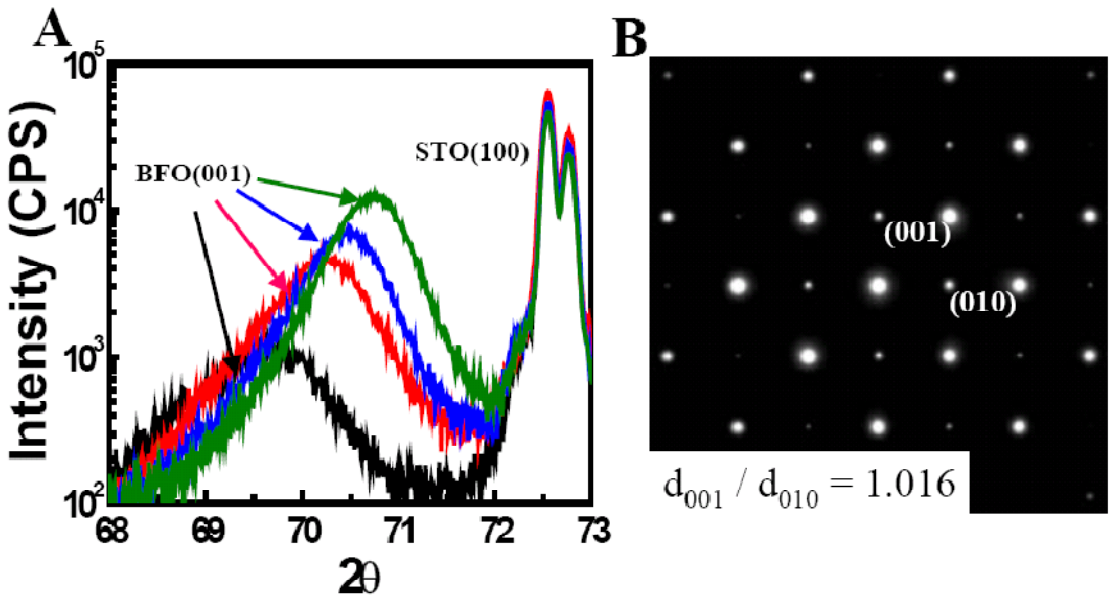
A
B
Intensity (CPS)
10^5
10^4
10^3
10^2
BFO(001)
STO(100)
68
69
70
71
72
73
2θ
(001)
(010)
d_{001} / d_{010} = 1.016

Fig. 1

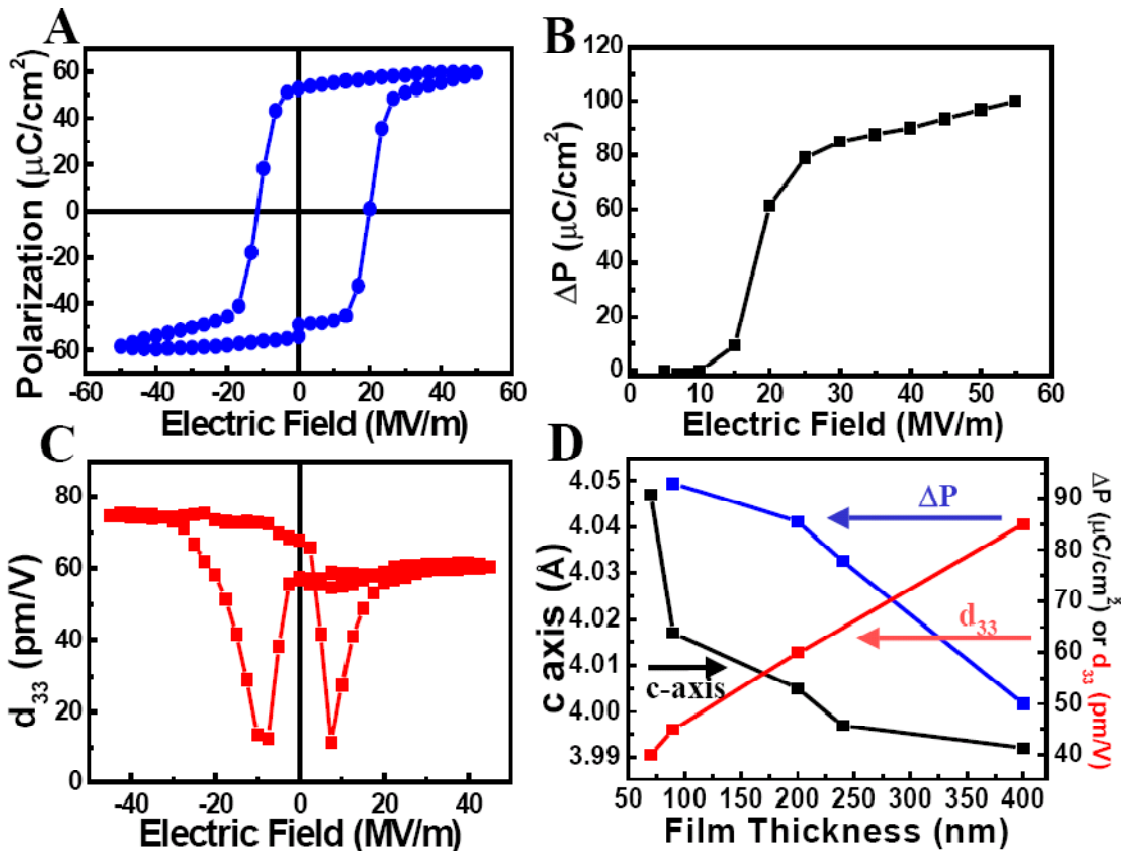
A
Polarization (μC/cm²)
Electric Field (MV/m)
B
ΔP (μC/cm²)
Electric Field (MV/m)
C
d33 (pm/V)
Electric Field (MV/m)
D
c axis (Å)
ΔP (μC/cm²) or d33 (pm/V)
ΔP
d33
c-axis
Film Thickness (nm)

Fig. 2

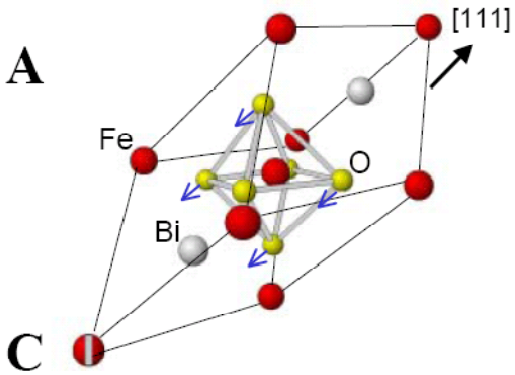

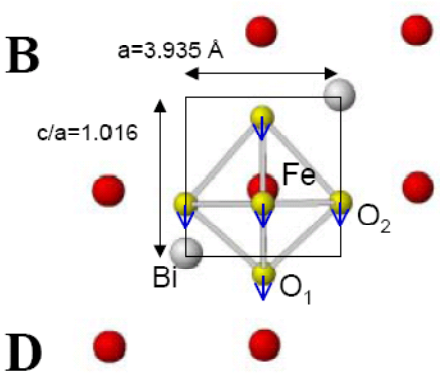

C

Rhombohedral R3c (P_s || [111])

	LSDA	Expt
Bi (2a) *x*	0	0
Fe (2a) *x*	0.2308	0.22077
O (6b) *x*	0.5423	0.5279
y	0.9428	0.9333
z	0.3980	0.3948
a (Å)	5.4590	5.6343
α (°)	60.36	59.348
V (Å^3)	115.98	124.601
P_s(μC/cm^2)	**6.61**	**6.1**

D

Tetragonal P4mm (P_s || [001])

	LSDA	Expt
Bi (1a) *z*	0	
Fe (1b) *z*	0.41	
O_1 (1b) *z*	-0.101	
O_2 (2c) *z*	0.367	
a (Å)	3.935*	3.935
c/a	1.016*	1.016
V (Å^3)	61.91*	61.91
P_s(μC/cm^2)	**63.2**	**50-60**

Fig. 3

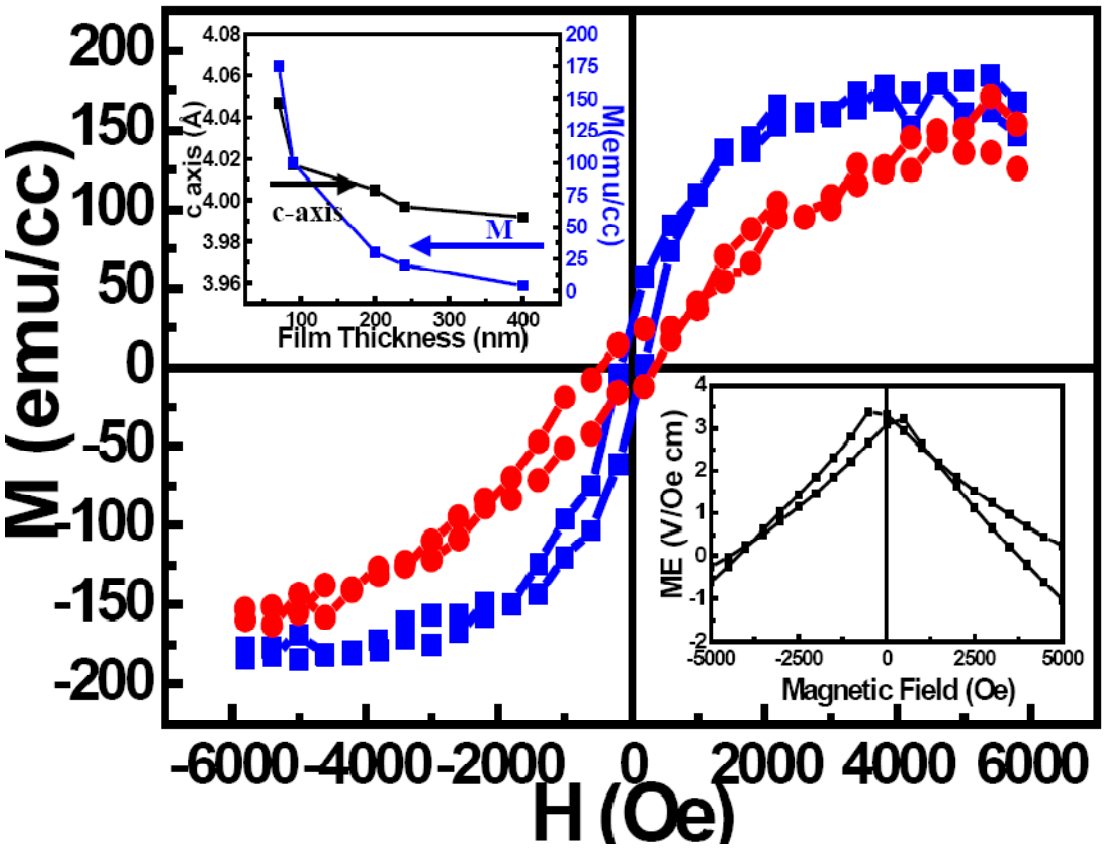
M (emu/cc)
H (Oe)
c axis (Å)
M(emu/cc)
c-axis
M
Film Thickness (nm)
ME (V/Oe cm)
Magnetic Field (Oe)

Fig. 4